Article

Modified Exp-Function Method to Find Exact Solutions of Microtubules Nonlinear Dynamics Models

Muhammad Shakeel [1,†], Attaullah [1], Nehad Ali Shah [2,†] and Jae Dong Chung [2,*]

1   Department of Mathematics, University of Wah, Wah Cantt., Rawalpindi 47040, Pakistan
2   Department of Mechanical Engineering, Sejong University, Seoul 05006, Republic of Korea
*   Correspondence: jdchung@sejong.ac.kr
†   These authors contributed equally to this work and are co-first authors.

Abstract: In this paper, we use the modified $\exp(-\psi(\theta))$-function method to observe some of the solitary wave solutions for the microtubules (MTs). By treating the issues as nonlinear model partial differential equations describing microtubules, we were able to solve the problem. We then found specific solutions to the nonlinear evolution equation (NLEE) covering various parameters that are particularly significant in biophysics and nanobiosciences. In addition to the soliton-like pulse solutions, we also find the rational, trigonometric, hyperbolic, and exponential function characteristic solutions for this equation. The validity of the method we developed and the fact that it provides more solutions are demonstrated by comparison to other methods. We next use the software Mathematica 10 to generate 2D, 3D, and contour plots of the precise findings we observed using the suggested technique and the proper parameter values.

Keywords: nonlinear model partial differential equation; analytical method; exact solutions; nonlinear evolution equation of microtubules

1. Introduction

Major cytoskeletal proteins are called microtubules (MTs). Cytoskeletal biopolymers called MTs are formed like nanotubes. They are proto-filaments (PFs), which are hollow cylinders made up of tubulin dimer-representing proteins. An electric dipole exists in every dimer. These dimers are either positioned straight inside the PFs or in radial positions that point outward from the cylindrical surface. MTs are an intriguing class of protein structures that could be used to create and build electronic nano-devices. Nonlinear partial differential equations (NPDEs) are used to simulate the dynamical behaviour of MTs. The physical conditions that arise in a variety of engineering disciplines, such as geochemistry, hydrodynamics, hydrodynamic plasma, solid state physics, optical fibres, hydrodynamic hydrodynamics, and others, and which are well described by fractional differential equations, are mathematically represented by these equations. The study of partial differential equations—specifically, those derived from finance mathematics—displays the elegance of symmetry analysis best. Symmetry is the key to nature; however, the majority of observations in the natural world lack symmetry. One method for hiding symmetry is the occurrence of spontaneous symmetry breakage. Finite and infinitesimal symmetries are the two categories under which they fall. For finite symmetries, discrete or continuous symmetries may exist. Space is a continuous transformation, whereas symmetry and time reverse are discrete natural symmetries. Numerous techniques have been used to solve NPDEs precisely or approximately up to now. These include, but are not restricted to, the rational perturbations technique [1], the Painlevé Expansion approach [2], Hirota's bi-linear approach [3], (G'/G)-growth approach [4,5], the F-expansion approach [6], the Jacobi elliptic function technique [7–9], Homogeneous Balance approach [10], the extended Tanh-function technique [11], the modified Tanh-function technique [12–15], the

$\exp(-\phi(\xi))$-expansion approach [16–22], the direct approach [23], the α-path method [24], the predictor-corrector method [25], the first hitting time method [26], the Fit clearance method [27], the approximation ratios method [28], and the chance-constrained support vector regression approach [29].

The purpose of this study is to use the modified exp-function method to create exact solutions for the following two NPDEs that mimic MT dynamics [30–38]. We specifically follow the initial setup given by Alam and Belgacem [38] when presenting the questions to be answered for comparative purposes, solving the Equations (1) and (2) by using the exp $(-\varphi(\xi))$-expansion method. Then, by employing an altogether different methodology, we deviate from their growth in a general way, though we nevertheless compare our results with those of [38] while bearing in mind the advancements in [36–38]. Table 1 compares the recently acquired solutions using current solutions found in the literature, indicating that our solutions are novel and preferred.

Table 1. Comparison of Solutions.

Our Solutions	Solutions by Alam and Belgacem [20]
If we put $B_0 = 1$, $B_1 = 0$, $a = \mu$, $b = \lambda$, $\theta = \xi$, and $u_1(x,t) = z_1(\xi)$ in our solution (18), then $z_1(\xi) = \sqrt{\frac{A}{B}} \{ A_0 - \beta \frac{2\mu}{\sqrt{\lambda^2+4\mu}\tanh\left(\frac{\sqrt{\lambda^2+4\mu}}{2}(\xi+E)\right)+\lambda} \}.$	If we put $\alpha = \beta$ in solution (24), then $z_1(\xi) = \sqrt{\frac{A}{B}} \{ A_0 - \beta \frac{2\mu}{\sqrt{\lambda^2+4\mu}\tanh\left(\frac{\sqrt{\lambda^2+4\mu}}{2}(\xi+E)\right)+\lambda} \}.$
If we put $B_0 = 1$, $B_1 = 0$, $a = \mu$, $b = \lambda$, $\theta = \xi$, and $u_2(x,t) = z_2(\xi)$ in our solution (19), then $z_2(\xi) = \sqrt{\frac{A}{B}} \{ A_0 + \beta \frac{2\mu}{\sqrt{4\mu-\lambda^2}\tan\left(\frac{\sqrt{4\mu-\lambda^2}}{2}(\xi+E)\right)-\lambda} \}.$	If we put $\alpha = \beta$ in solution (25), then $z_2(\xi) = \sqrt{\frac{A}{B}} \{ A_0 + \beta \frac{2\mu}{\sqrt{4\mu-\lambda^2}\tan\left(\frac{\sqrt{4\mu-\lambda^2}}{2}(\xi+E)\right)-\lambda} \}.$
If we put $B_0 = 1$, $B_1 = 0$, $a = \mu$, $b = \lambda$, $\theta = \xi$, and $u_3(x,t) = z_3(\xi)$ in our solution (20), then $z_3(\xi) = \sqrt{\frac{A}{B}} \{ A_0 + \beta \left(\frac{\lambda}{\exp(\lambda(\xi+E))-1} \right) \}.$	If we put $\alpha = \beta$ in solution (26), then $z_3(\xi) = \sqrt{\frac{A}{B}} \{ A_0 + \beta \left(\frac{\lambda}{\exp(\lambda(\xi+E))-1} \right) \}.$
If we put $B_0 = 1$, $B_1 = 0$, $a = \mu$, $b = \lambda$, $\theta = \xi$, and $u_4(x,t) = z_4(\xi)$ in our solution (21), then $z_4(\xi) = \sqrt{\frac{A}{B}} \{ A_0 - \beta \left(\frac{\lambda^2(\xi+E)}{2((\lambda(\xi+E))+2)} \right) \}.$	If we put $\alpha = \beta$ in solution (27), then $z_4(\xi) = \sqrt{\frac{A}{B}} \{ A_0 - \beta \left(\frac{\lambda^2(\xi+E)}{2((\lambda(\xi+E))+2)} \right) \}.$
If we put $B_0 = 1$, $B_1 = 0$, $a = \mu$, $b = \lambda$, $\theta = \xi$, and $u_5(x,t) = z_5(\xi)$ in our solution (22), then $z_5(\xi) = \sqrt{\frac{A}{B}} \{ A_0 + \beta \left(\frac{1}{(\xi+E)} \right) \}.$	If we put $\alpha = \beta$ in solution (28), then $z_5(\xi) = \sqrt{\frac{A}{B}} \{ A_0 + \beta \left(\frac{1}{(\xi+E)} \right) \}.$
If we put $B_0 = 1$, $B_1 = 0$, $a = \mu$, $b = \lambda$, $\theta = \xi$, and $u_6(x,t) = z_6(\xi)$ in our solution (28), then $z_6(\xi) = \sqrt{6} \{ A_0 - \frac{2T}{3} \left(\frac{2\mu}{\sqrt{\lambda^2+4\mu}\tanh\left(\frac{\sqrt{\lambda^2+4\mu}}{2}(\xi+E)\right)+\lambda} \right) \}.$	If we put $z_1(x,t) = z_6(\xi)$ in solution (41), then $z_6(\xi) = \sqrt{6} \{ A_0 - \frac{2T}{3} \left(\frac{2\mu}{\sqrt{\lambda^2+4\mu}\tanh\left(\frac{\sqrt{\lambda^2+4\mu}}{2}(\xi+E)\right)+\lambda} \right) \}.$
If we put $B_0 = 1$, $B_1 = 0$, $a = \mu$, $b = \lambda$, $\theta = \xi$, and $u_7(x,t) = z_7(\xi)$ in our solution (29), then $z_7(\xi) = \sqrt{6} \{ A_0 + \frac{2T}{3} \left(\frac{2\mu}{\sqrt{4\mu-\lambda^2}\tan\left(\frac{\sqrt{4\mu-\lambda^2}}{2}(\xi+E)\right)-\lambda} \right) \}.$	If we put $z_2(x,t) = z_7(\xi)$ in solution (41), then $z_7(\xi) = \sqrt{6} \{ A_0 + \frac{2T}{3} \left(\frac{2\mu}{\sqrt{4\mu-\lambda^2}\tan\left(\frac{\sqrt{4\mu-\lambda^2}}{2}(\xi+E)\right)-\lambda} \right) \}.$
If we put $B_0 = 1$, $B_1 = 0$, $a = \mu$, $b = \lambda$, $\theta = \xi$, and $u_8(x,t) = z_8(\xi)$ in our solution (30), then $z_8(\xi) = \sqrt{6} \{ A_0 + \frac{2T}{3} \left(\frac{\lambda}{\exp(\lambda(\xi+E))-1} \right) \}.$	If we put $z_3(x,t) = z_8(\xi)$ in solution (43), then $z_8(\xi) = \sqrt{6} \{ A_0 + \frac{2T}{3} \left(\frac{\lambda}{\exp(\lambda(\xi+E))-1} \right) \}.$
If we put $B_0 = 1$, $B_1 = 0$, $a = \mu$, $b = \lambda$, $\theta = \xi$, and $u_9(x,t) = z_9(\xi)$ in our solution (31), then $z_9(\xi) = \sqrt{6} \{ A_0 - \frac{2T}{3} \left(\frac{\lambda^2(\xi+E)}{2((\lambda(\xi+E))+2)} \right) \}.$	If we put $z_4(x,t) = z_9(\xi)$ in solution (44), then $z_9(\xi) = \sqrt{6} \{ A_0 - \frac{2T}{3} \left(\frac{\lambda^2(\xi+E)}{2((\lambda(\xi+E))+2)} \right) \}.$
If we put $B_0 = 1$, $B_1 = 0$, $a = \mu$, $b = \lambda$, $\theta = \xi$, and $u_{10}(x,t) = z_{10}(\xi)$ in our solution (32), then $z_{10}(\xi) = \sqrt{6} \{ A_0 + \frac{2T}{3} \left(\frac{1}{(\xi+E)} \right) \}.$	If we put $z_5(x,t) = z_{10}(\xi)$ in solution (45), then $z_{10}(\xi) = \sqrt{6} \{ A_0 + \frac{2T}{3} \left(\frac{1}{(\xi+E)} \right) \}.$

(i) The nonlinear PDE describes the model of microtubule nonlinear dynamics assum-ing a single longitudinal degree of freedom per tubulin dimer (see [38]),

$$m\frac{\partial^2 H\,(x,t)}{\partial\,t^2} - k\,L^2\,\frac{\partial^2 H\,(x,t)}{\partial\,x^2} - Q\,E - A\,H\,(x,t) + B\,H^3\,(x,t) + \gamma\frac{\partial H\,(x,t)}{\partial\,t} = 0, \quad (1)$$

Q is the additional charge inside the dipole, L for MT length, m is the mass to the dimer, $H(x,t)$ is the travelling wave, E is the strength of the intrinsic electronic field, γ is the coefficient of viscosity, and k is a harmonic variable that describes the nearest-neighbour interactions among dimers of the same kind proto-filaments, and A, B are the nonnegative parameters. The exact solutions of Equation (1) were discovered using the Jacobi elliptic function approach in [39], the physical details and derivations of which were covered there but omitted here for simplicity.

(ii) The nonlinear PDE explaining the radially displaced MTs' nonlinear dynamics:

$$I\frac{\partial^2 H(x,t)}{\partial\,t^2} - k\,l^2\,\frac{\partial^2 H(x,t)}{\partial\,x^2} + p\,E\,H(x,t) - \frac{p\,E}{6}H^3(x,t) + \Gamma\frac{\partial H\,(x,t)}{\partial\,t} = 0, \quad (2)$$

where I is the solitary dimer's moment of inertia, Γ is the coefficient of viscosity, l is for MT length, p is the strength of the intrinsic electronic field, k denotes the inter-dimer bond formation interaction between PFs, and $H(x,t)$ as the whole dimer rotates, is the equivalent angular displacement.

The structure of this article is as follows: We describe the modified $\exp(-\psi(\theta))$-function method in Section 2 and use it to solve the given NPDEs (1) and (2), in Section 3. Physical justifications are provided in Section 4, and the conclusion is presented in Section 5. An extensive list of references is provided at the end of the article for readers who may be interested.

2. The Portrayal of the Method

Consider the general NLPDE of the form

$$F(H,\ H_x,\ H_t,\ H_{x\,x},\ H_{t\,t},\ H_{t\,x},\ldots) = 0, \quad (3)$$

where H is an undisclosed function and F is a polynomial in H with partial derivatives that contain nonlinear terms and higher order derivatives. The key stages in using this technique are listed in [40]:

Stage 1: The following travelling transformation is defined as follows:

$$H(x,t) = u(\theta),\ \theta = (k_1\,x + k_2\,t\,), \quad (4)$$

where k_1 and k_2 are the constants, representing wave velocity and frequency, respectively.

Equation (3) can be transformed into a nonlinear ODE by using Equation (4):

$$T\left(u, k_1 u', k_2^2 u'',\ldots\right) = 0, \quad (5)$$

where T is a polynomial in u and its ordinary derivatives and ''' denotes the usual derivatives with regard to θ.

Stage 2: Assume that the following expression can be used to represent the travelling wave solution of Equation (5):

$$u(\theta) = \frac{\sum_{i=0}^{M} A_i[\exp(-\Psi(\theta))]^i}{\sum_{j=0}^{N} B_j[\exp(-\Psi(\theta))]^j} = \frac{A_0 + A_1\exp(-\Psi(\theta)) + \ldots + A_M\exp(M(-\Psi(\theta)))}{B_0 + B_1\exp(-\Psi(\theta)) + \ldots + B_N\exp(N(-\Psi(\theta)))}, \quad (6)$$

where $\Psi = \Psi(\theta)$ satisfy the following ODE, and A_i, B_j, $(0 \le i \le M$, $0 \le j \le N,)$ stay the variables that will be determined later, so that $A_M \ne 0$, $B_N \ne 0$:

$$\Psi'(\theta) = \exp(-\Psi(\theta)) + a \exp(\Psi(\theta)) + b, \tag{7}$$

where a and b are constants.

The following solution sets exist for Equation (7): a

a. When $a \ne 0$, $b^2 - 4a > 0$,

$$\Psi(\theta) = \ln\left(\frac{-\sqrt{b^2 - 4a}}{2a} \tanh\left(\frac{\sqrt{b^2 - 4a}}{2} (\theta + E) \right) - \frac{b}{2a} \right). \tag{8}$$

b. When $a \ne 0$, $b^2 - 4a < 0$,

$$\Psi(\theta) = \ln\left(\frac{\sqrt{-b^2 + 4a}}{2a} \tan\left(\frac{\sqrt{-b^2 + 4a}}{2} (\theta + E) \right) - \frac{b}{2a} \right). \tag{9}$$

c. When $a = 0$, $b \ne 0$, $b^2 - 4a > 0$,

$$\Psi(\theta) = -\ln\left(\frac{b}{\exp(b(\theta + E)) - 1} \right). \tag{10}$$

d. When $a \ne 0$, $b \ne 0$, $b^2 - 4a = 0$,

$$\Psi(\theta) = -\ln\left(-\frac{2b(\theta + E) + 4}{b^2(\theta + E)} \right). \tag{11}$$

e. When $b = 0$, $a = 0$, $b^2 - 4a = 0$,

$$\Psi(\theta) = \ln(\theta + E). \tag{12}$$

Such that A_0, A_1, A_2, ... A_M, B_0, B_1, B_2, ... B_N, E, a, b are later-to-be-calculated constants. We may determine the positive integers M and N by employing the notion of homogenous balancing between both the highest order linear term and the highest order nonlinear term found in Equation (6).

Stage 3: Using Maple 18, we can solve the system of algebraic equations to find the values of the unknowns. This is done by substituting the Equations (7)–(12) into the Equation (6). This results in a polynomial in various powers of the $\exp(-\Psi(\theta))$ and equating all the coefficients to zero. The generic solutions of Equation (6) complete the strength of the solution of Equation (1) by substituting the values of the unknown constants.

3. Applications

The modified exp-function method, which includes a new complex and a hyperbolic function solution, will be used to provide new analytical solutions for the nonlinear PDE dynamical Equations (1) and (2) of motion in this phase. Equation (1) is transformed into the following NLODE by the travelling wave variable Equation (5).

$$P\, u''(\theta) - Q\, u'(\theta) - u(\theta) + u^3(\theta) - R = 0, \tag{13}$$

where $P = \frac{m\,\omega^2 - k\,l^2 k_1^2}{A}$, $Q = \frac{\gamma\,\omega}{A}$, $R = \frac{q\,E}{A\sqrt{A/B}}$, $H(\theta) = \sqrt{\frac{A}{B}}\, u(\theta)$.

The relationship between u^3 and u'' is defined by the balance principle as the following equation:

$$M = N + 1. \tag{14}$$

Applying this connection, we can achieve the following new analytical solutions such as Equation (1):

Let us say $N = 1$ and $M = 2$, then Equation (6) becomes

$$u = \frac{A_0 + A_1 \exp(-\Psi) + A_2 \exp(2(-\Psi))}{B_0 + B_1 \exp(-\Psi)}, \tag{15}$$

in which $A_2 \neq 0$ and $B_1 \neq 0$. We attain a polynomial containing $\exp(-\Psi(\theta))$ and all of its powers by substituting Equations (7) and (15) into Equation (13). The coefficients of the polynomial of $\exp(-\Psi(\theta))$ then give us a system of algebraic equations. The following values for the various coefficients are obtained after this system has been resolved using Maple 18.

Case 1:

$$\begin{aligned}
R &= \frac{1}{27} \frac{Q\,(2\,Q^2 + 9\,P)\beta}{P^2} \,, \quad a = \frac{1}{18} \frac{3\beta\,Q\,A_0\,B_0 + 2\,Q^2 B_0^2 - 9\,P\,A_0^2 + 9\,P\,B_0^2}{P^2\,B_0^2} \,, \\
b &= -\frac{1}{3} \frac{3\beta A_0 + B_0 Q}{P\,B_0}, \; A_0 = A_0, \; A_1 = \frac{\beta\,B_0^2 + A_0\,B_1}{B_0} \,, \; A_2 = \beta\,B_1 \,,
\end{aligned} \tag{16}$$

where A_0, P and, Q are arbitrary constants and $\beta = \pm\sqrt{-2\,p}$.

We derived the following travelling wave solutions for Equation (1) by substituting Equations (8)–(12) and the coefficient values from Equation (16) into Equation (15) as seen below:

When $a \neq 0$, $b^2 - 4a > 0$,

$$H_1(x,t) = \sqrt{\frac{A}{B}} \left(\frac{3\tanh[f(x,t)]PA_0\sqrt{-3Q^2 + 18P} + 3PQA_0 - B_0\sqrt{-P}(2\sqrt{2}Q^2 - 9P)}{3P\left(\sqrt{-3Q^2 + 18P}\tanh[f(x,t)]B_0 - 3\sqrt{-2P}A_0 - B_0Q\right)} \right), \tag{17}$$

where $f(x,t) = \frac{1}{6}\sqrt{-\frac{3Q^2 + 18P}{P^2}}(\theta + E)$.

When $a \neq 0$, $b^2 - 4a < 0$,

$$H_2(x,t) = \sqrt{\frac{A}{B}} \left(-\frac{-3\tan[g(x,t)]\sqrt{3}PA_0\sqrt{Q^2 + 6P} + 3PQA_0 - B_0\sqrt{-2P}(2Q^2 - 9P)}{3P\left(\sqrt{3}\sqrt{Q^2 + 6P}\tan[g(x,t)]B_0 + 3\sqrt{-2P}A_0 + B_0Q\right)} \right), \tag{18}$$

where $g(x,t) = \frac{1}{2\sqrt{3}}\sqrt{\frac{Q^2 + 6P}{P^2}}(\theta + E)$.

When $a = 0$, $b \neq 0$, $b^2 - 4a > 0$,

$$H_3(x,t) = \sqrt{\frac{A}{B}} \left(\frac{3\exp\left(-\frac{(3\sqrt{-2P}A_0 + B_0Q)(\theta + E)}{3PB_0}\right)PA_0 + 9PA_0 - 2\sqrt{-2P}QB_0}{PB_0\left(\exp\left(-\frac{(3\sqrt{-2P}A_0 + B_0Q)(\theta + E)}{3PB_0}\right) - 1\right)} \right). \tag{19}$$

When $a \neq 0$, $b \neq 0$, $b^2 - 4a = 0$,

$$H_4(x,t) = \sqrt{\frac{A}{B}} \left(-\frac{\left(-\frac{3A_0\sqrt{-2P} + B_0Q}{PB_0}\right)^2 B_0(\theta + E)\sqrt{-2P} - 2A_0\left((-3A_0\sqrt{-2P} + B_0Q)(\theta + E) + 2PB_0\right)}{2B_0\left((-3A_0\sqrt{-2P} + B_0Q)(\theta + E) + 2PB_0\right)} \right). \tag{20}$$

When $a = 0$, $b = 0$, $b^2 - 4a = 0$,

$$H_5(x,t) = \sqrt{\frac{A}{B}} \left(\frac{B_0\sqrt{-2P} + A_0(\theta + E)}{B_0(\theta + E)} \right). \tag{21}$$

where $\theta = (k_1\,x + k_2\,t)$, E is an arbitrary constant.

The exact solutions to Equation (2) are found in this subsection. To this goal, we reduce Equation (2) to the following NLODE using the transformation Equation (4).

$$S\, u''(\theta) - T\, u'(\theta) - u^3(\theta) + u(\theta) = 0, \tag{22}$$

where $S = \frac{I\,\omega^2 - k\,l^2 k_1^2}{p\,E}$, $T = \frac{\Gamma\,\omega}{p\,E}$, $H(\theta) = \sqrt{6}\,u(\theta)$.

The relationship between u^3 and u'' is defined by the balance principle as the following equation:

$$M = N + 1. \tag{23}$$

Applying this relationship, we can obtain a variety of novel analytical solutions for Equation (2), as shown below:

Let us say $N = 1$ and $M = 2$, and we can write

$$u = \frac{A_0 + A_1 \exp(-\Psi) + A_2 \exp(2(-\Psi))}{B_0 + B_1 \exp(-\Psi)}, \tag{24}$$

such that $A_2 \neq 0$, and $B_1 \neq 0$, while b and a are arbitrary constants. We get the coefficient values listed below after using Maple 18 to resolve this system:

Case 2:

$$S = \frac{2}{9}T^2,\ a = \frac{9\,A_0^2 \pm 9\,A_0\,B_0}{4T^2\,B_0^2},\ b = \frac{\mp 6\,A_0 - 3\,B_0}{2T\,B_0},\ A_0 = A_0, A_1 = \frac{\mp 2\,T\,B_0^2 + 3A_0\,B_1}{3B_0},\ A_2 = \mp\frac{2}{3}T\,B_1. \tag{25}$$

where A_0 and T are arbitrary constants.

We obtain the following travelling wave solutions for the Equation (2) by substituting Equations (8)–(12) and the coefficient values from Equation (25) into Equation (15) as follows:

When $a \neq 0$, $b^2 - 4a > 0$,.

$$H_6(x,t) = \sqrt{6}\left(\frac{A_0\left(\tanh\left(\frac{3(\theta+E)}{4T}\right) \pm 1\right)}{\tanh\left(\frac{3(\theta+E)}{4T}\right)B_0 \mp 2A_0 - B_0}\right). \tag{26}$$

When $a \neq 0$, $b^2 - 4a < 0$,

$$H_7(x,t) = \sqrt{6}\left(\frac{A_0\left(\tan\left(\frac{3}{4}\sqrt{-\frac{1}{T^2}}(\theta+E)\right)i - 1\right)}{\tan\left(\frac{3}{4}\sqrt{-\frac{1}{T^2}}(\theta+E)\right)iB_0 \pm 2A_0 + B_0}\right). \tag{27}$$

When $a = 0$, $b \neq 0$, $b^2 - 4a > 0$,

$$H_8(x,t) = \sqrt{6}\left(\frac{\exp\left(\mp\frac{3(2A_0 \pm B_0)(\theta+E)}{2TB_0}\right)A_0 + 3A_0 \pm 2B_0}{B_0\left(\exp\left(\mp\frac{3(2A_0 \pm B_0)(\theta+E)}{2TB_0}\right) - 1\right)}\right). \tag{28}$$

When $a \neq 0$, $b \neq 0$, $b^2 - 4a = 0$,

$$H_9(x,t) = \sqrt{6}\left(\frac{\left(\left(\pm 3(E+\theta)B_0^2 + 12\left(E + \frac{2}{3}T + \theta\right)A_0B_0 \pm 12A_0^2(\theta+E)\right)(\theta+E) - 6A_0B_0\right) \mp 12A_0^2}{2B_0(4T(\theta+E)B_0 \mp 6A_0 - 3B_0)}\right). \tag{29}$$

When $a = 0$, $b = 0$, $b^2 - 4a = 0$,

$$H_{10}(x,t) = \sqrt{6}\left(\frac{3(\theta+E)A_0 \mp 2TB_0}{3B_0(\theta+E)}\right). \tag{30}$$

where $\theta = (k_1\,x + k_2\,t)$, E is an arbitrary constant.

4. Physical Expression of the Problem

The modified exp-function method's key characteristics are presented in this part, along with the physical significance of the novel hyperbolic, trigonometric, and exponential and rational function solutions produced by applying the modified exp-function method to Equations (1) and (2).

According to the exp-$(-\psi(\theta))$-expansion approach, the modified exp-function method is more extensive because it has an additional parameter named *N*. As indicated by the fact that we have obtained so many analytical solutions to the equations under discussion for only *N* = 1 and *M* = 2, this results in a large number of coefficients, which leads to a large number of travelling wave solutions. To the best of our knowledge, some of these analytical solutions, such as Equations (17)–(21) and (26)–(30), are published in the literature for the first time when they are compared with solutions derived by Alam and Belgacem [39].

If we ponder *N* = 2 and *M* = 3, then we may write

$$u = \frac{A_0 + A_1 \exp{(-\Psi)} + A_2 \exp{(2(-\Psi))} + A_3 \exp{(3(-\Psi))}}{B_0 + B_1 \exp{(-\Psi)} + B_2 \exp{(2(-\Psi))}}, \tag{31}$$

where $A_3 \neq 0$, $B_2 \neq 0$. The coefficients of the polynomial of exp-$(-\psi(\theta))$ yield a system of algebraic equations when Equation (31) is substituted into Equations (13) and (22). We can discover more different-style analytical solutions to this problem using Maple 18, which are not possible by relying solely on the exp-$(-\psi(\theta))$-expansion method. In order to achieve more analytical solutions, a better knowledge of engineering and physical problems, along with novel physical predictions, Equation (6)'s technique will help. In short, different *M* and *N* numbers can lead to additional analytical solutions for the problem under consideration. This leads to additional analytical solutions with novel physical meaning and properties.

Secondly, circular functions include hyperbolic tangent functions. They appear in a variety of mathematical physics and math problems. For instance, the computation and speed of special relativity give rise to the hyperbolic tangent. In general relativity, these can be seen in the Schwarzschild metric with external isotropic Kruskal coordinates [41].

By choosing certain values for parameters and visualizing the precise solutions obtained by the mathematical program Mathematica 10 (Figures 1–10), we observe the characteristics of several solutions to the microtubule model as nonlinear dynamics of radially displaced particles. As a result of those research findings, we showed that Equations (17)–(21) and (26)–(30) exhibit kink solutions, periodic solutions, as well as singular solitons solutions and singular kink solutions.

Graphical representations are a great way to discuss and illustrate solutions to problems in a straightforward and understandable scheme. A graph is a graphical representation of quantitative and qualitative responses and perhaps additional data that can be easily compared. After doing calculations, we need to gain a fundamental understanding of the graphs. Equation (18) serves as a representation of a kink wave solution. Kink waves are those that tour between two asymptotic states. The kink solution becomes constant at infinity. Figure 1 displays the 2D, 3D, and contour plots of $H_1(x,t)$, such as unidentified constants, $A_0 = 1$, $B_0 = -1$, $k_1 = 2$, $k_2 = -1$, $\beta = 1$, $Q = 2$, $A = 2$, $B =3$, $E = 1$ within $-10 \leq x, t \leq 10$ such as 3D and $t = 2$ thus 2D graphs. The precise periodic travelling wave solution is denoted by Equation (19). A travelling wave solution with a periodic profile, such as cos(*x-t*), is known as a periodic wave. Figure 2 represents 2D, 3D, and contour graphs of $H_2(x,t)$ thus $A_0 = 1$, $B_0 = 2$, $k_1 = 2$, $k_2 = -1$, $\beta = 1$, $Q = -6$, $A = 2$, $B = 3$, $E = 5$ within $-3 \leq x, t \leq 3$ thus the 3D and $t = 1$ thus 2D graphs. Figure 3 shows the singular kink type wave solution profile of $H_3(x,t)$ such as $A_0 = 1$, $B_0 = -1$, $k_1 = 2$, $k_2 = -1$, $\beta = 1$, $Q = 2$, $A = 2$, $B = 3$, $E = 1$ within $-5 \leq x$, $t \leq 5$ such as 3D and contour graphs and $t = 1$ thus 2D graph. Figure 4 characterizes the singular soliton-type solution of $H_4(x,t)$ such as $A_0 = 1$, $B_0 = -2$, $B_1 = 1$, $k_1 = 2$, $k_2 = 1$, $\beta = 1$, $Q = 6$, $A = 2$, $B = 3$, $E = 5$ within $-12 \leq x, t \leq 12$ for 3D and contour graphs and $t = 1$ for 2D graph. Figure 5 illustrates the rational function of $H_5(x,t)$ that behave likewise to bright singular soliton solution such as $A_0 = 1$, $B_0 = 0.2$, $k_1 = 2$, $k_2 = 1$, $\beta = 1$, $A = 2$,

$B = 3$, $E = 5$ and within $-15 \leq x, t \leq 15$ thus the 3D graphs and $t = 1$ thus 2D graph. The hyperbolic function solution $H_6(x, t)$ in Equation (28) behaves like a kink-type solution for $A_0 = 1$, $B_0 = 2$, $k_1 = 1$, $k_2 = -1$, $T = 1$, $E = 1$ and within $-10 \leq x, t \leq 10$, thus 3D plots and $t = 1$ thus 2D graph are shown in Figure 6. The solution $H_7(x, t)$ in Figure 7 establishes the periodic soliton solution for $A_0 = 1$, $B_0 = -5$, $k_1 = 2$, $k_2 = -1$, $T = 1$, $E = 1$ in the limit, $-5 \leq x, t \leq 5$, thus 3D graphs and $t = 1$ thus 2D diagram. Figure 8 signifies the singular kink-type soliton solution of Equation (30) for $A_0 = 1$, $B_0 = -1$, $k_1 = 1$, $k_2 = -1$, $T = 1.5$, $E = 1$ and in the limit, $-5 \leq x, t \leq 5$, thus 3D graphs and $t = 1$ thus 2D diagram. Figure 9 demonstrates the exact travelling wave solution of $H_9(x, t)$ for $A_0 = -10$, $B_0 = -10$, $k_1 = 1$, $k_2 = -10$, $T = 5$, $E = 5$, for 3D and contour graphs within the range $-2 \leq x, t \leq 2$, and $t = 1$ as 2D graph. Figure 10 denotes the multiple singular soliton trajectory to such as $A_0 = 1$, $B_0 = 0.2$, $B_1 = -1$, $k_1 = 1$, $k_2 = 1$, $T = 2$, $E = 5$ thus 3D graphs and $t = 0.5$ thus the 2D graph through the limit $-5 \leq x, t \leq 5$.
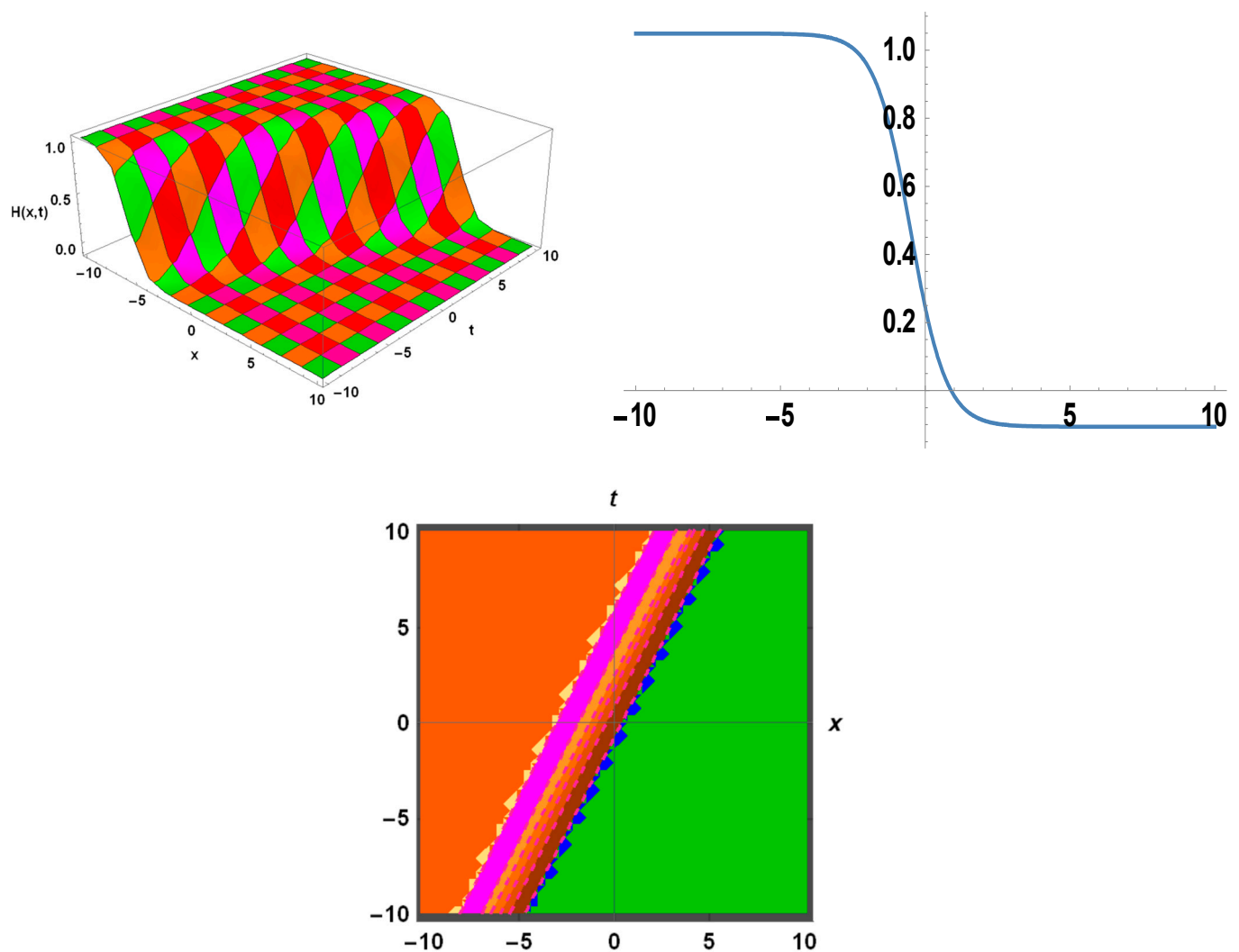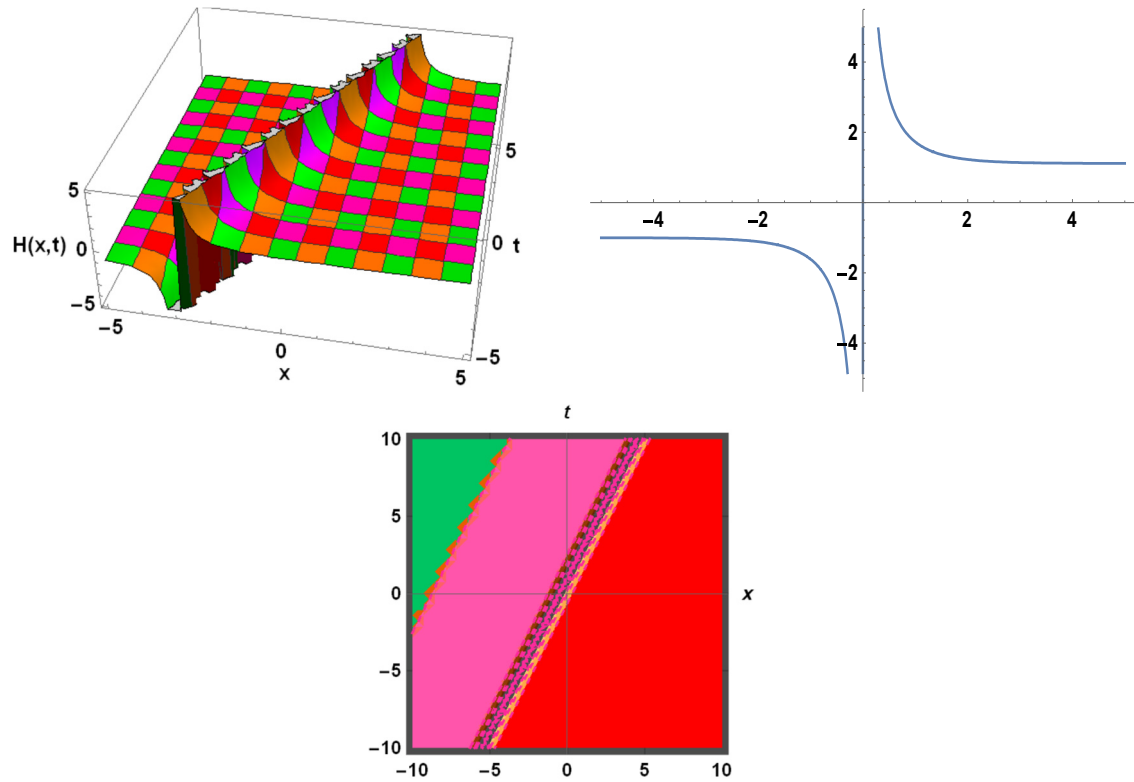

Figure 1. The graphical view of $H_1(x, t)$ for various values of parameters.
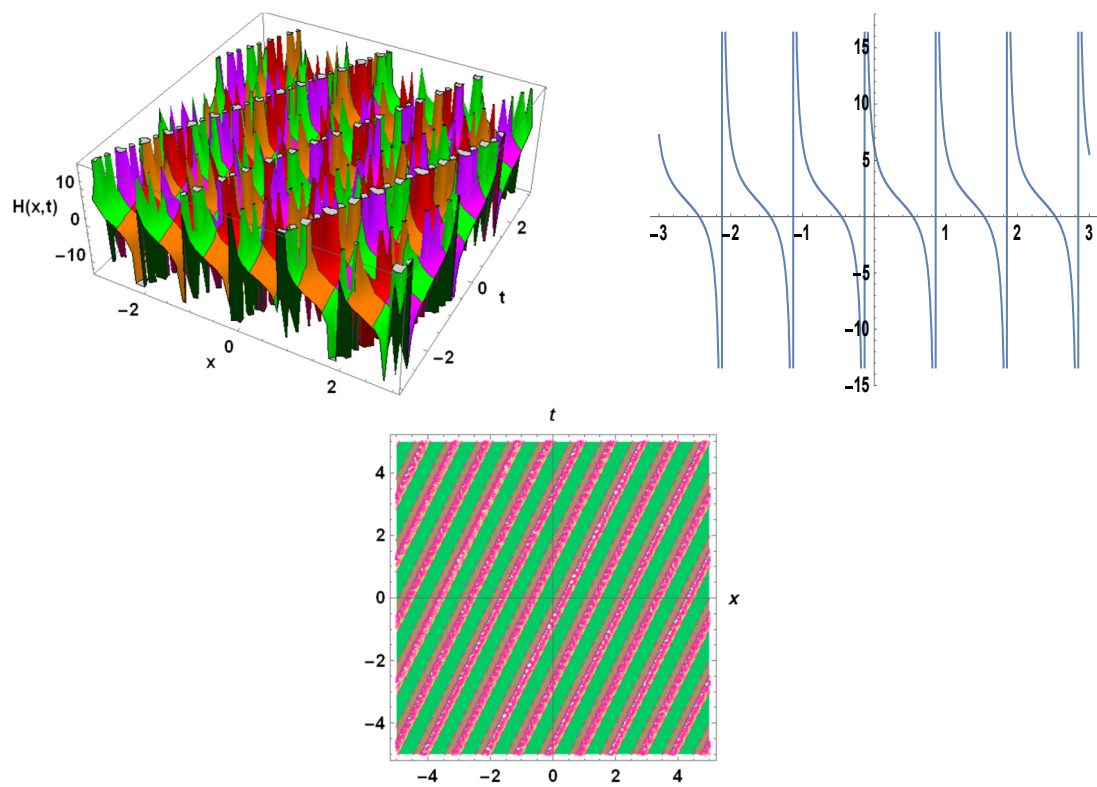
Figure 2. The graphical view of $H_2(x, t)$ for various values of parameters.

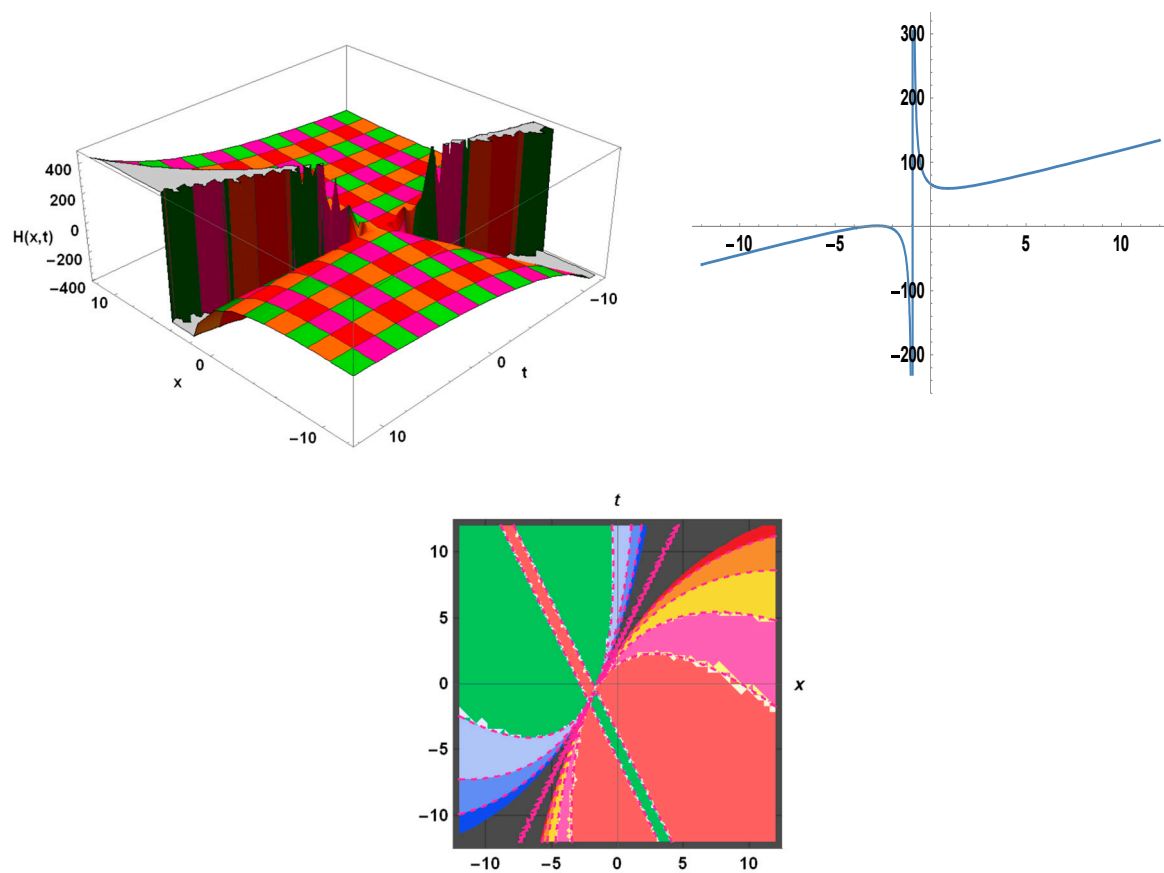**Figure 3.** The graphical view of $H_3(x, t)$ for various values of parameters.

Figure 4. The graphical view of $H_4(x, t)$ for various values of parameters.
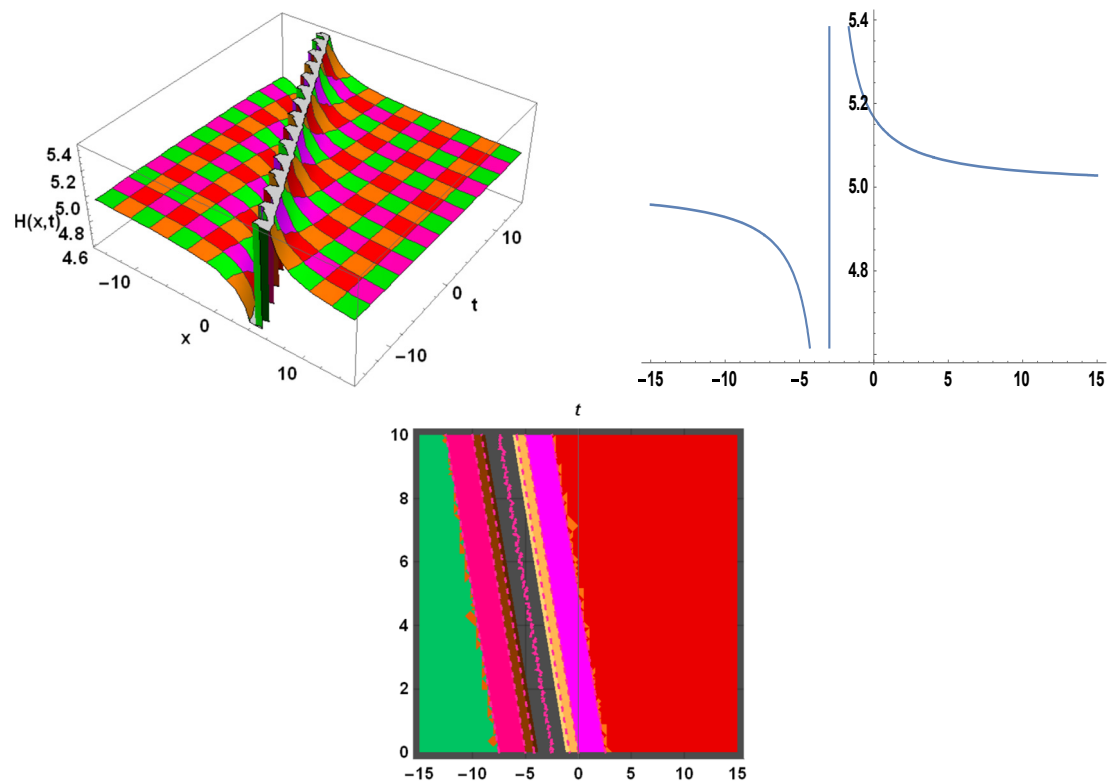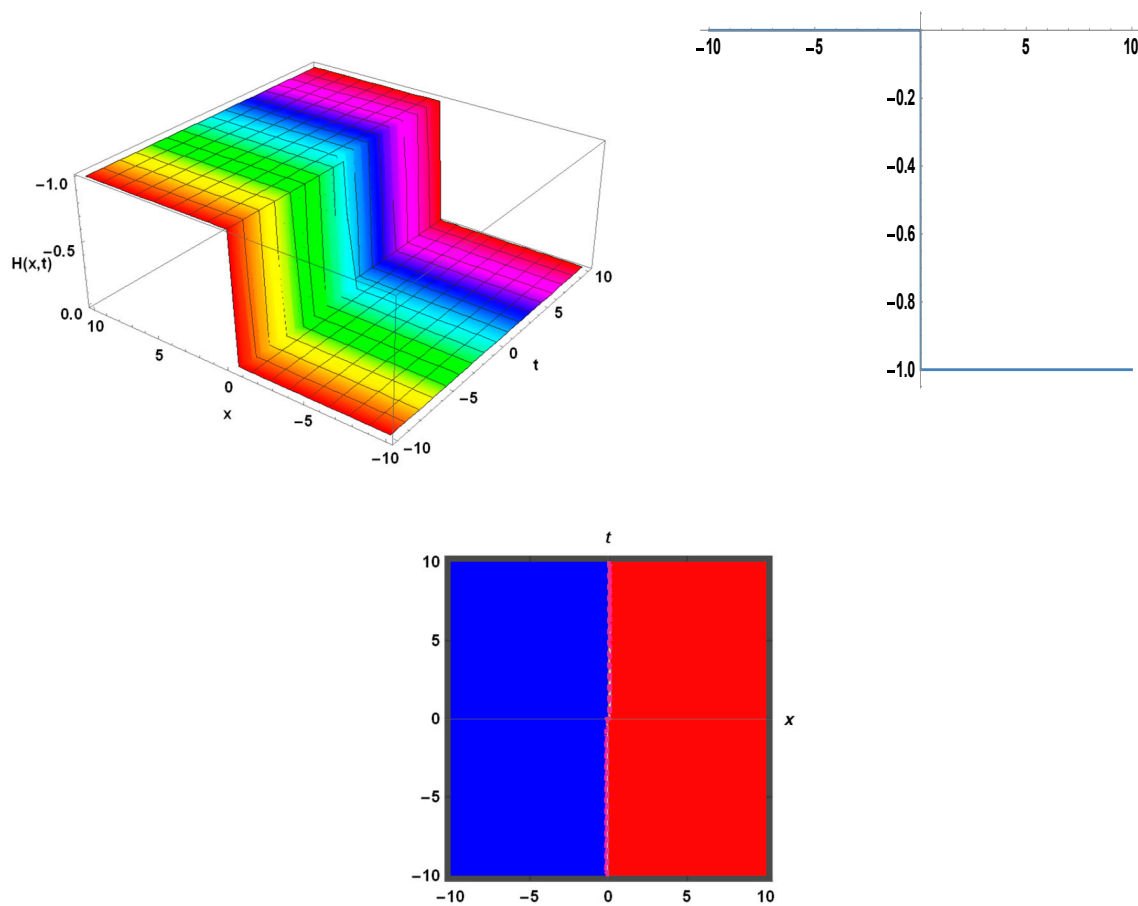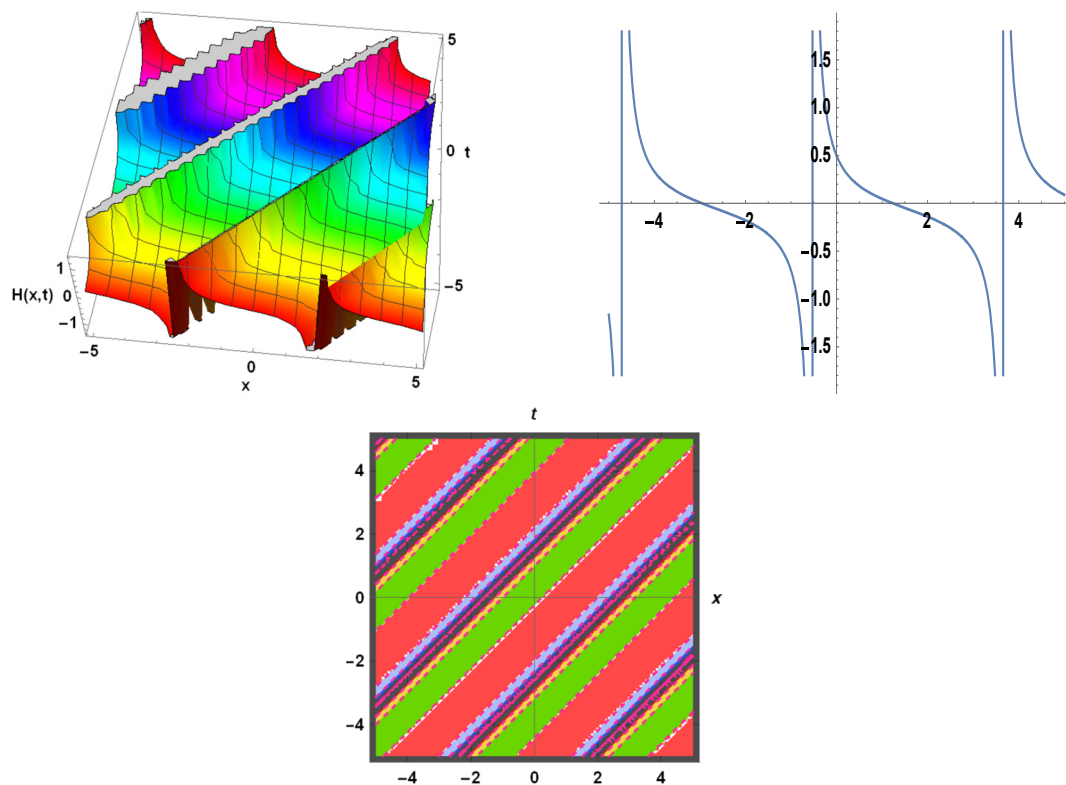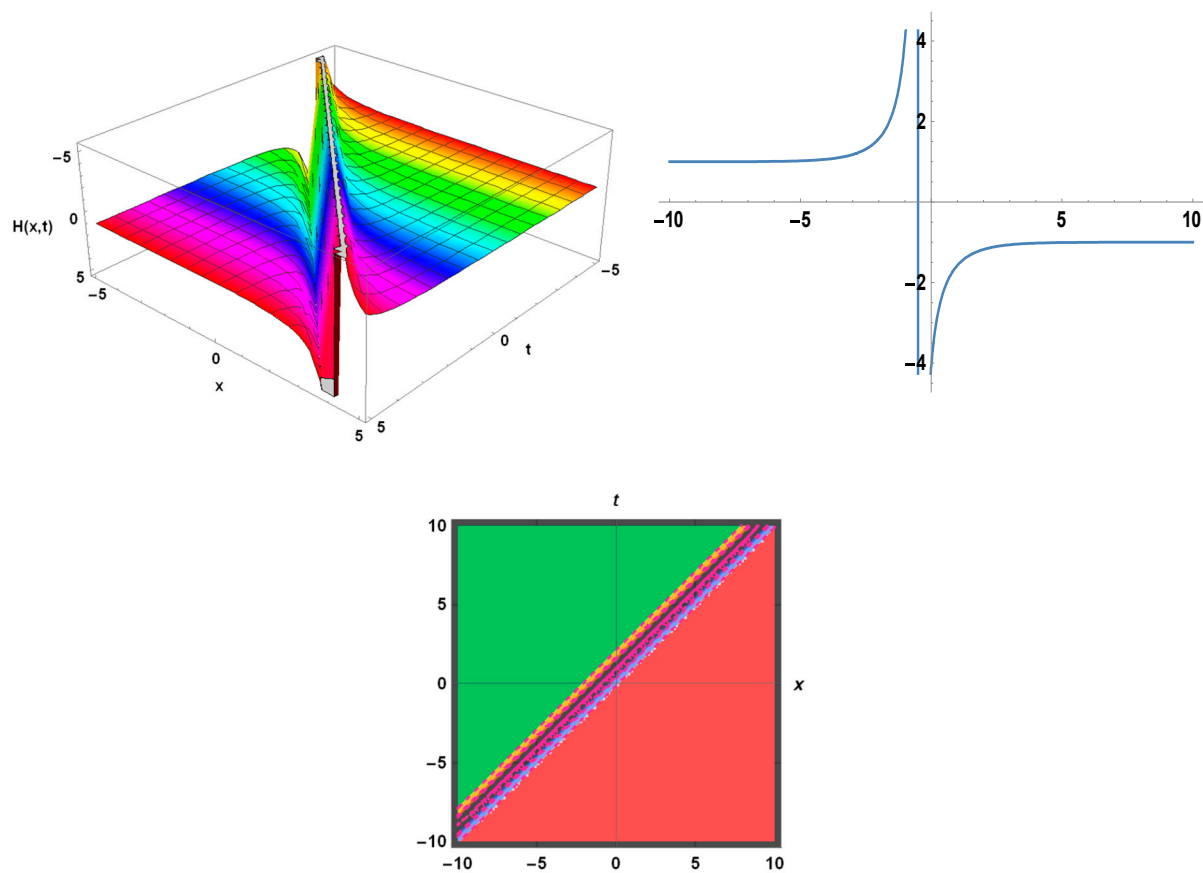

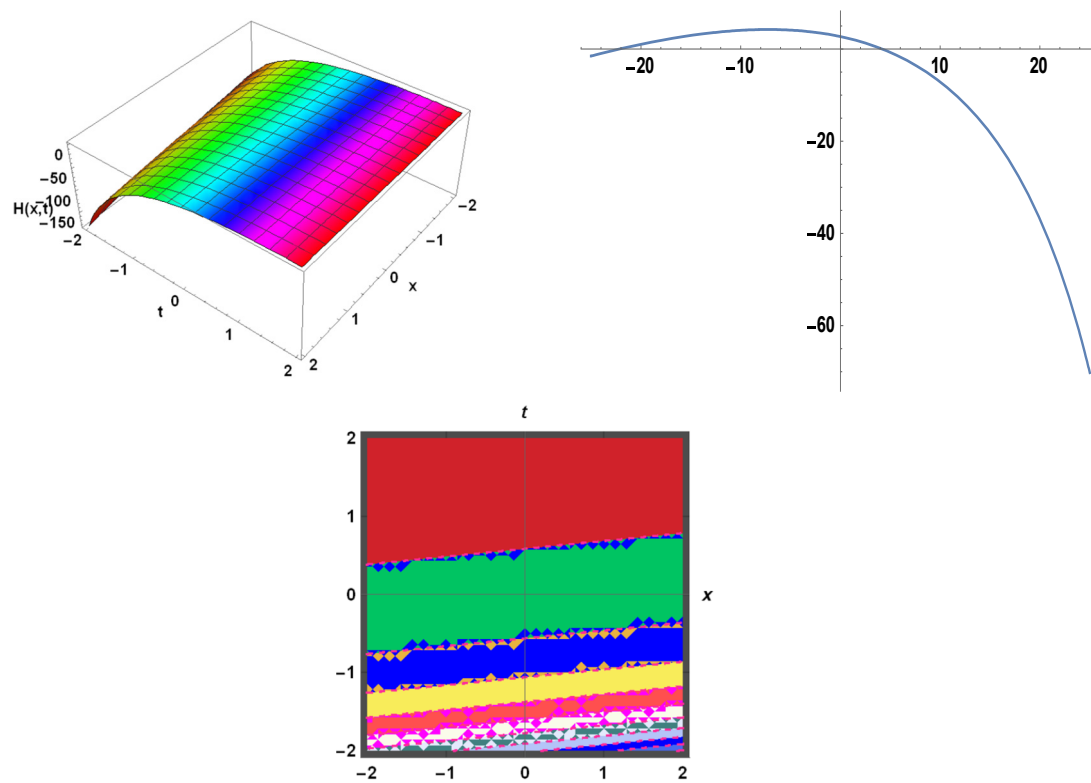**Figure 5.** The graphical view of $H_5(x, t)$ for various values of parameters.

Figure 6. The graphical view of $H_6(x, t)$ for various values of parameters.

Figure 7. The graphical view of $H_7(x, t)$ for various values of parameters.

Figure 8. The graphical view of $H_8(x, t)$ for various values of parameters.

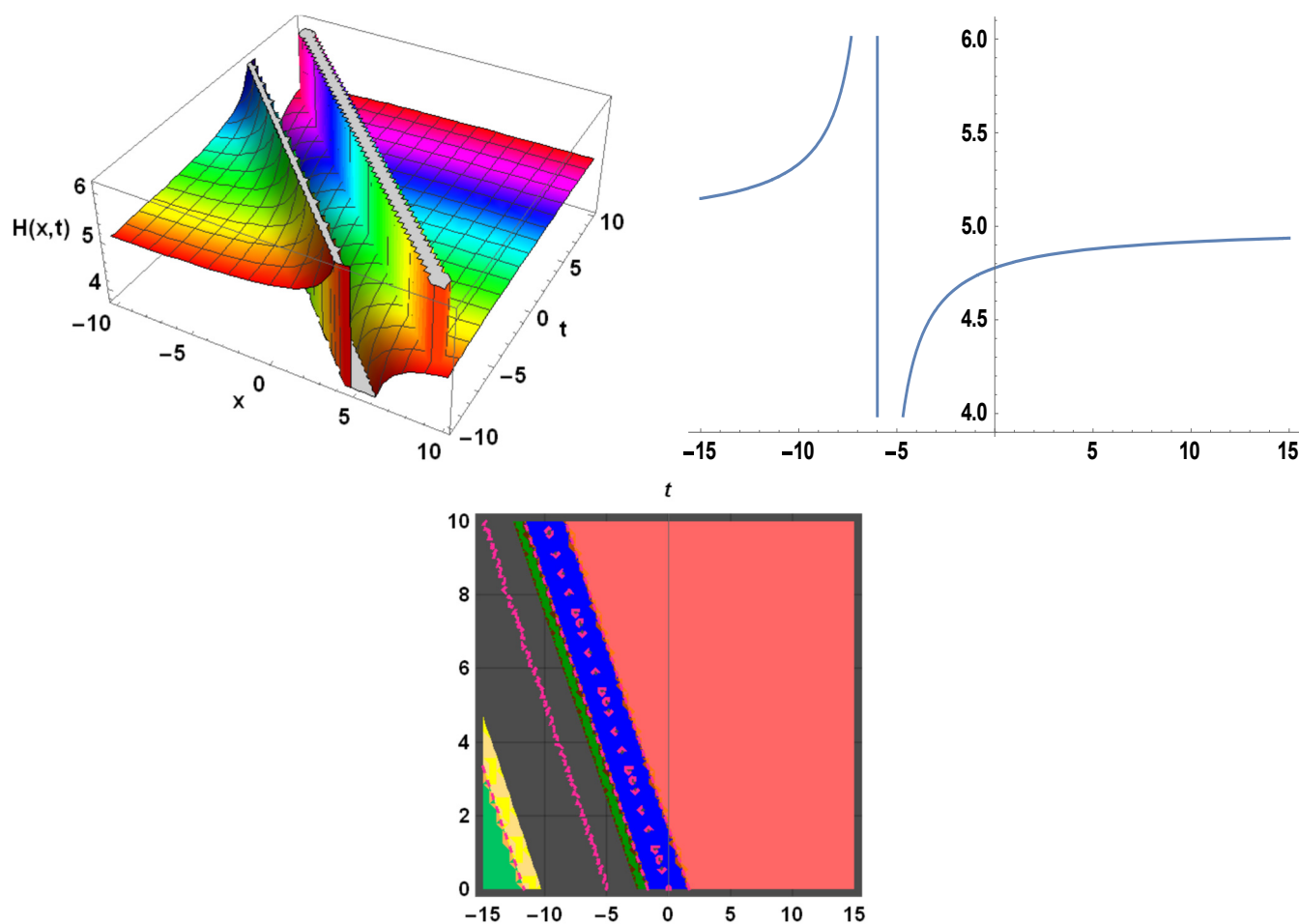**Figure 9.** The graphical view of $H_9(x, t)$ for various values of parameters.

Figure 10. The graphical view of $H_{10}(x,t)$ for various values of parameters.

5. Conclusions

We were able to conduct analytical and numerical research on the propagation of soliton-like signals in microtubules by modelling them as nonlinear model partial differential equation equations. These models are built using the structure of the proteins that make up microtubules. With the usage of the modified exp-function technique, a novel analytical solution, including the solitary wave solutions shown in Figures 1–10, have been made possible. Here, the best in the case of positive integer numbers $M = 2$ for $N = 1$ has been taken into consideration. More standard results will be obtained if $M = 3$ is kept in mind for $N = 2$, indicating the originality of our study. All of the exact solutions found in this research to the nonlinear model partial differential equation modelling microtubules version were verified using Maple 18 and were found to be accurate. This method worked well to generate fresh analytical approaches to solitary wave solutions found in Figures 1–10. It has been established that the used approach is efficient because it offers numerous cutting-edge solutions. In addition, we plotted the received solutions in 3D, 2D, and contour graphs. In this study, we found solutions for trigonometric, hyperbolic, exponential, and rational functions. Additionally, we created a Table 1 to compare the solutions we came up with to those found in the literature. When parameters are specified, all of the solutions from Table 1 must be invented.

Conflicts of Interest: The declare no conflict of interest.

References

1. Jafar, B.; Asadi, M.A.; Salehi, F. Rational Homotopy Perturbation Method for solving stiff systems of ordinary differential equations. *Appl. Math. Model.* **2015**, *39*, 1291–1299.
2. Cariello, F.; Tabor, M. Painlevé expansions for nonintegrable evolution equations. *Phys. D Nonlinear Phenom.* **1989**, *39*, 77–94. [CrossRef]
3. Philip, D.G.; Drazin, P.G.; Johnson, R.S. *Solitons: An Introduction*; No. 2; Cambridge University Press: Cambridge, UK, 1989.
4. Aslam, M.N.; Akbar, M.A.; Mohyud-Din, S.T. General traveling wave solutions of the strain wave equation in microstructured solids via the new approach of generalized (G′/G)-expansion method. *Alex. Eng. J.* **2014**, *53*, 233–241. [CrossRef]
5. Shakeel, M.; Ul-Hassan, Q.M.; Ahmad, J.; Naqvi, T. Exact solutions of the time fractional BBM-Burger equation by novel (G′/G)-expansion method. *Adv. Math. Phys.* **2014**, *2014*, 181594. [CrossRef]
6. Zhou, Y.; Wang, M.; Wang, Y. Periodic wave solutions to a coupled KdV equations with variable coefficients. *Phys. Lett. A* **2003**, *308*, 31–36. [CrossRef]
7. Ali, A.T. New generalized Jacobi elliptic function rational expansion method. *J. Comput. Appl. Math.* **2011**, *235*, 4117–4127. [CrossRef]
8. Lü, D. Jacobi elliptic function solutions for two variant Boussinesq equations. *Chaos Solitons Fractals* **2005**, *24*, 1373–1385. [CrossRef]
9. Liu, S.; Fu, Z.; Liu, S.; Zhao, Q. Jacobi elliptic function expansion method and periodic wave solutions of nonlinear wave equations. *Phys. Lett. A* **2001**, *289*, 69–74. [CrossRef]
10. Fan, E. Two new applications of the homogeneous balance method. *Phys. Lett. A* **2000**, *265*, 353–357. [CrossRef]
11. Fan, E. Extended tanh-function method and its applications to nonlinear equations. *Phys. Lett. A* **2000**, *277*, 212–218. [CrossRef]
12. Soliman, A.A. The modified extended tanh-function method for solving Burgers-type equations. *Phys. A Stat. Mech. Its Appl.* **2006**, *361*, 394–404. [CrossRef]
13. Li, Z.; Liu, Y. RATH: A Maple package for finding travelling solitary wave solutions to nonlinear evolution equations. *Comput. Phys. Commun.* **2002**, *148*, 256–266. [CrossRef]
14. Peng, Y.Z. A mapping method for obtaining exact travelling wave solutions to nonlinear evolution equations. *Chin. J. Phys.* **2003**, *41*, 103–110.
15. Yomba, E. Construction of new soliton-like solutions of the (2+ 1) dimensional dispersive long wave equation. *Chaos Solitons Fractals* **2004**, *20*, 1135–1139. [CrossRef]
16. Alam, N.; Alam, M.M. An analytical method for solving exact solutions of a nonlinear evolution equation describing the dynamics of ionic currents along microtubules. *J. Taibah Univ. Sci.* **2017**, *11*, 939–948. [CrossRef]
17. MAlam, N.; Hafez, M.G.; Akbar, M.A.; Roshid, H.O. Exact traveling wave solutions to the (3+1)-dimensional mKdV-ZK and the (2+1)-dimensional Burgers equations via exp (-Eta)-expansion method. *Alex. Eng. J.* **2015**, *54*, 635–644.
18. Roshid, H.O.; Alam, M.N.; Akbar, M.A. Traveling wave solutions for fifth order (1+1)-dimensional Kaup-Keperschmidt equation with the help of exp(−Φ(ξ))-expansion method. *Walailak J. Sci. Technol.* **2015**, *12*, 1063–1073.
19. Alam, M.N.; Hafez, M.G.; Akbar, M.A.; Roshid, H.O. Exact solutions to the (2+1)-dimensional Boussinesq equation via exp(−Φ(ξ))-expansion method. *J. Sci. Res.* **2015**, *7*, 1–10. [CrossRef]
20. Alam, M.N.; Belgacem, F.B.M. Microtubules nonlinear models dynamics investigations through the exp(−Φ(ξ))-expansion method implementation. *Mathematics* **2016**, *4*, 6. [CrossRef]
21. Shakeel, M.; Mohyud-Din, S.T.; Iqbal, M.A. Closed form solutions for coupled nonlinear Maccari system. *Comput. Math. Appl.* **2018**, *76*, 799–809. [CrossRef]
22. Liu, H.-Z. An equivalent form for the exp(−Φ(ξ))-expansion method. *Jpn. J. Ind. Appl. Math.* **2018**, *35*, 1153–1161. [CrossRef]
23. Jeffrey, A.; Mohamad, M.N.B. Exact solutions to the KdV-Burgers' equation. *Wave Motion* **1991**, *14*, 369–375. [CrossRef]
24. Jin, T.; Yang, X. Monotonicity theorem for the uncertain fractional differential equation and application to uncertain financial market. *Math. Comput. Simul.* **2021**, *190*, 203–221. [CrossRef]
25. Jin, T.; Yang, X.; Xia, H.; Ding, H. Reliability index and option pricing formulas of the first hitting time model based on the uncertain fractional-order differential equation with Caputo type. *Fractals* **2021**, *29*, 2150001. [CrossRef]
26. Tian, C.; Jina, T.; Yang, X.; Liu, Q. Reliability analysis of the uncertain heat conduction model. *Comput. Math. Appl.* **2022**, *119*, 131–140. [CrossRef]
27. Bai, X.; Shi, H.; Zhang, K.; Zhang, X.; Wu, Y. Effect of the fit clearance between ceramic outer ring and steel pedestal on the sound radiation of full ceramic ball bearing system. *J. Sound Vib.* **2022**, *529*, 116967. [CrossRef]

28. Li, S.; Liu, Z. Scheduling uniform machines with restricted assignment. *Math. Biosci. Eng.* **2022**, *19*, 9697–9708. [CrossRef]
29. Shao, Z.; Zhai, Q.; Han, Z.; Guan, X. A linear AC unit commitment formulation: An application of data-driven linear power flow model. *Int. J. Electr. Power Energy Syst.* **2023**, *145*, 108673. [CrossRef]
30. Sataric, M.V.; Sekulic, D.L.; Sataric, B.M.; Zdravkovic, S. Role of nonlinear localized Ca^{2+} pulses along microtubules in tuning the mechano-Sensitivity of hair cells. *Prog. Biophys. Mol. Biol.* **2015**, *119*, 162–174. [CrossRef]
31. Sekulic, D.; Sataric, M.V. An improved nanoscale transmission line model of microtubules: The effect of nonlinearity on the propagation of electrical signals. *Facta Univ. Ser. Electron. Energ.* **2015**, *28*, 133–142. [CrossRef]
32. Sekulic, D.L.; Sataric, B.M.; Tuszynski, J.A.; Sataric, M.V. Nonlinear ionic pulses along microtubules. *Eur. Phys. J. E Soft Matter* **2011**, *34*, 49. [CrossRef] [PubMed]
33. Sekulic, D.; Sataric, M.V.; Zivanov, M.B. Symbolic computation of some new nonlinear partial differential equations of nanobio-sciences using modified extended tanh-function method. *Appl. Math. Comput.* **2011**, *218*, 3499–3506. [CrossRef]
34. Sataric, M.V.; Sekulic, D.; Zivanov, M.B. Solitonic ionic currents along microtubules. *J. Comput. Theor. Nanosci.* **2010**, *7*, 2281–2290. [CrossRef]
35. Zayed, E.M.E.; Alurrfi, K.A.E. The generalized projective Riccati equations method and its applications for solving two nonlinear PDEs describing microtubules. *Int. J. Phys. Sci.* **2015**, *10*, 391–402.
36. Sekulic, D.L.; Sataric, M.V. Microtubule as Nanobioelectronic nonlinear circuit. *Serb. J. Electr. Eng.* **2012**, *9*, 107–119. [CrossRef]
37. Zdravkovic, S.; Sataric, M.V.; Maluckov, A.; Balaz, A. A nonlinear model of the dynamics of radial dislocations in microtubules. *Appl. Math. Comput.* **2014**, *237*, 227–237. [CrossRef]
38. Zdravkovic, S.; Sataric, M.V.; Zekovic, S. Nonlinear dynamics of microtibules-A longitudinal model. *Europhys. Lett.* **2013**, *102*, 38002. [CrossRef]
39. Zekovic, S.; Muniyappan, A.; Zdravkovic, S.; Kavitha, L. Employment of Jacobian elliptic functions for solving problems in nonlinear dynamics of microtubules. *Chin. Phys. B* **2015**, *23*, 020504. [CrossRef]
40. Shakeel, M.; Iqbal, M.A.; Din, Q.; Hassan, Q.M.; Ayub, K. New exact solutions for coupled nonlinear system of ion sound and Langmuir waves. *Indian J. Phys.* **2020**, *94*, 885–894. [CrossRef]
41. Weisstein, E.W. *Concise Encyclopedia of Mathematics*, 2nd ed.; CRC: New York, NY, USA, 2002.